Statistics of Small-Scale Velocity Fluctuations and Internal Intermittency in Marine Stratocumulus Clouds

H. SIEBERT

Leibniz Institute for Tropospheric Research, Leipzig, Germany

R. A. SHAW

Leibniz Institute for Tropospheric Research, Leipzig, Germany, and Department of Physics, Michigan Technological University, Houghton, Michigan

Z. WARHAFT

Mechanical and Aerospace Engineering, Cornell University, Ithaca, New York

(Manuscript received 20 May 2009, in final form 20 July 2009)

ABSTRACT

Clouds are known to be turbulent, but the details of their internal turbulent structure have been largely unexplored. Measurements of turbulent velocities in stratocumulus clouds presented here reveal an intermittent structure consistent with that observed in classic homogeneous isotropic turbulence. The measurements were taken close to cloud top in a 200-m-thick cloud layer over a path of approximately 6 km, using a hot-wire anemometer below a helicopter as part of the Airborne Cloud Turbulence Observation System (ACTOS) measurement system. Hot-wire signal artifacts resulting from droplet impacts are removed without significantly degrading the signal, such that high-order velocity structure functions can be evaluated. The structure function analysis for orders 2–8 show statistically significant departures from the Kolmogorov's 1941 scaling, yielding scaling exponents consistent with the Kolmogorov–Obukhov refined similarity hypothesis, with an intermittency exponent of 0.25. This is in agreement with the accepted value determined in single-phase flows under carefully controlled conditions, and no evidence is found of any departure from the large body of knowledge obtained from the laboratory on the finescale turbulence structure. This suggests that processes depending on the finescale structure of turbulence that cannot presently be measured in clouds can be explored in the laboratory setting. Since these findings pertain to clouds with relatively low liquid water content and weak turbulence, further work will be required to determine their applicability to other cloud types.

1. Introduction

In the atmosphere, turbulence plays a dominant role in scalar transport and mixing, pollutant dispersion, and boundary layer growth (Wyngaard 2010). For example, the transport of scalars by turbulence is greater than the transport due to molecular diffusion by approximately the order of the Reynolds number. Typical atmospheric Reynolds numbers ($\mathrm{Re} = lu'/\nu$) are in the range 10^6–10^8 based on the characteristic eddy scale (l), the rms turbulent velocity (u'), and the kinematic air viscosity (ν). Most clouds are highly turbulent, with characteristic Reynolds numbers in the same range or higher than those observed in the boundary layer (Siebert et al. 2006b), yet measuring the details of their turbulence structure has remained a challenge. Entrainment, mixing, transport, droplet size distribution, and droplet growth in clouds are all affected by turbulence, but the mechanisms and the degree to which turbulence plays a role are poorly understood (Shaw 2003). A precursor to such understanding depends on the measurement of the underlying turbulent field itself. It has been suggested, for example, that the small-scale structure of turbulence in clouds can be strongly modified as a result of phase changes (Malinowski et al. 2008; Korczyk et al. 2006), and it is widely known that turbulence can be influenced simply by the presence of a dispersed material

Corresponding author address: Holger Siebert, Leibniz Institute for Tropospheric Research, Permoserstr. 15, 04318 Leipzig, Germany.
E-mail: siebert@tropos.de

DOI: 10.1175/2009JAS3200.1

if the mass loading is sufficiently large (e.g., Crowe et al. 1997; Tanaka and Eaton 2008).[1] The statistical properties of statistically homogeneous, isotropic turbulence are well characterized and measured (e.g., Sreenivasan and Antonia 1997), so it would be advantageous to know how cloud turbulence differs from that classical picture. It is the purpose of this paper to present measurements of the small-scale structure of the turbulence field inside a cloud, and to compare these measurements with what is known from laboratory studies, and from measurements in the clear atmosphere. At present, there are no experimental results for the intermittency and higher-order velocity structure functions in clouds.

Intermittency effects in turbulence play a major role in high Reynolds number turbulence, causing regions of greatly enhanced dissipation and mixing. Laboratory measurements in shear and unsheared flows (Anselmet et al. 1984; Mydlarski and Warhaft 1996), as well as atmospheric measurements in clear air (Praskovsky and Oncley 1994; Muschinski et al. 2004), show that while the turbulence structure is approximately Gaussian at the large scale, at the small scales it is strongly intermittent and non-Gaussian. Thus, velocity derivatives, which emphasize the fluctuating gradients at the dissipation scales, have probability density functions with stretched exponential tails, although the signal itself is Gaussian. There is a gradual increase in the non-Gaussian nature of the velocity field as the velocity increments become smaller and smaller in the inertial subrange. The long-tailed probability density functions (pdf's) indicate that rare events are many times more probable than for a Gaussian-distributed variable with equal variance. Consistent with Kolmogorov similarity hypotheses (Frisch 1995), the intermittency becomes more pronounced with increasing Reynolds number but its characteristics in the inertial and dissipation subranges are found to be independent of the way the turbulence is forced. Thus, higher-order structure function exponents are similar in jets, wakes, boundary layers (including that of the atmosphere), and decaying grid-generated turbulence (Sreenivasan and Antonia 1997; Jiang et al. 2006).

The intermittency at the inertial and dissipation scales is thought to be due to intense small-scale structures (Frisch 1995; Ishihara et al. 2009) but there are still uncertainties concerning the dynamics. For example, the relative importance of the cascade from the large to the small scales, to that of direct large-scale–small-scale interaction, is not well understood. Direct large-scale–small-scale interaction is responsible for intermittency in the scalar field (Shraiman and Siggia 2000; Warhaft 2000), a problem that is more tractable than that of the velocity field itself. While most of our evidence for the intermittent nature of the velocity field has come from hot-wire measurements at a point in the flow (Eulerian measurements), during the past decade Lagrangian laboratory measurements (Toschi and Bodenschatz 2009) have shown that the particle acceleration trajectories also exhibit intense intermittency, resulting in accelerations tens and sometimes hundreds of times greater than that due to gravity, and increasing with Reynolds number. Are the turbulence characteristics different in clouds or can we extend the knowledge and tools developed from laboratory and theoretical research to cloud problems? The answer is of considerable importance in understanding the potential impacts of turbulence on mixing and droplet growth, and may give some indication as to how the droplets modify the turbulence, if at all.

The lack of data on the turbulence structure in clouds is due to the extreme difficulty in making the measurements. Early detailed measurements of turbulence and turbulent transport in the boundary layer were achieved by placing probes on towers (Haugen 1973), a technique that cannot be used for cloud studies (except perhaps for fog events or low clouds). Obtaining high-resolution turbulence data from aircraft is difficult because of the extremely high sampling frequencies needed to resolve the submillimeter structures at the dissipation scale, due to the high true airspeed. Further, hot wires, still the preferred method for high-resolution turbulence measurements, are fragile, particularly in the hostile, two-phase flow of clouds, and the drops impinging on the hot wires cause spikes in the data that require careful postprocessing. Recently, Siebert et al. (2007) developed a method for overcoming these problems and have shown in wind-tunnel experiments that for low droplet concentration and low flow speeds hot wires can be used for high-resolution measurements in two-phase flows. Some turbulence characteristics have been measured with an ultrasonic anemometer (~15 cm resolution), including spectra and dissipation rates, in a cloudy boundary layer (Siebert et al. 2006b). In that work, a tethered balloon was employed, a method that alleviates the resolution problem, but that approach is inappropriate for the heights and agility needed to explore a broader range of clouds.

Here, we employ a system in which a hot-wire anemometer is suspended with other turbulence and cloud probes, from a helicopter well below the effects of the helicopter rotor wake (Siebert et al. 2006a). The helicopter-borne measurement payload, known as the Airborne

[1] At several recent international cloud physics meetings, prominent individuals have made public statements that cloud turbulence is completely unlike single-phase laboratory turbulence. While such remarks are qualitative, they provide a sense of the fundamental uncertainty that is widespread in the field.

Cloud Turbulence Observation System (ACTOS), allows us to reach appropriate cloud locations meeting the required conditions and, in contrast to airborne measurements, does not require very fast sampling rates. Because of the low speed, we were able to deploy a hot-wire anemometer and record velocity fluctuations with high temporal resolution. Furthermore, the data were taken in stratocumulus clouds, which allow for long, continuous data records under statistically homogeneous conditions—a requirement for calculating higher-order statistics. The aim of this work, then, is to use these high-resolution measurements to investigate the intermittent character of small-scale turbulence in a cloud and to compare these results to what is observed in well-controlled laboratory experiments. Our study, the first of this nature, takes place under the relatively calm conditions of a stratocumulus cloud with low droplet concentrations; it therefore represents one type of cloud and, in the future, measurements will need to be extended to other conditions.

2. Background

Small-scale turbulence is often described in terms of the statistics of velocity fluctuations, $u'(x) \equiv u(x) - \langle u \rangle$ (where the angle brackets indicate an average), or the statistics of velocity increments, $\Delta u(r, x) \equiv u'(x + r) - u'(x)$. Here, we have reduced the problem to one dimension where x is the space parameter along the flight path and $u(x)$ is the longitudinal component of the velocity vector $[u(x), v(x), w(x)]$ in a right-handed system. The shapes of the pdf's of u' and Δu are of key importance. As mentioned, the pdf's of the velocity increments have stretched exponential tails in laboratory turbulence, reflecting the increased probability of rare events in comparison with Gaussian distributions with the same variance.

Another tool often used to analyze the statistics and correlation of velocity increments is the nth-order structure function $S^{(n)}(r)$, which is defined as

$$S^{(n)}(r) \equiv \langle [\Delta u(r)]^n \rangle_x. \tag{1}$$

Here, $\langle \cdot \rangle_x$ denotes an ensemble average over the measurement path. Classical turbulence theory (Kolmogorov 1941, hereafter K41) predicts for statistical homogeneous and isotropic turbulence a scaling behavior like $S^{(n)}(r) \sim r^{\zeta_n}$ with a scaling exponent $\zeta_n = n/3$ (e.g., Davidson 2004; Frisch 1995). In practice, the velocity is sampled with a hot wire as a function of time t and, assuming the validity of Taylor's hypotheses of ''frozen turbulence,'' the spatial lag r can be transformed from a temporal lag $r = t'U$ with the average aircraft speed U (relative to the environmental air, also called true airspeed). The classical scaling behavior of $S^{(n)}(r)$ results in two important relations often used to estimate the energy dissipation rate ε in a turbulent flow (e.g., Frisch 1995):

$$S^{(2)}(r) \simeq 2(\varepsilon r)^{2/3}, \tag{2}$$

and, for third-order statistics,

$$S^{(3)}(r) = \frac{4}{5}\varepsilon r. \tag{3}$$

At high Reynolds numbers, the energy dissipation rate is intermittent, with large regions of relatively low dissipation and rare bursts of intense dissipation. Accounting for this intermittency via the refined similarity hypothesis (Kolmogorov 1962, hereafter K62) leads to a modified form for the structure functions of $S^{(n)}(r) \sim r^{\zeta'_n}$. The scaling exponent has the form $\zeta'_n = n/3 - \mu n(n - 3)/18$, with an intermittency factor of $\mu \approx 0.25$ (e.g., Pope 2000; Davidson 2004). Thus, the exponents ζ'_n are reduced with increasing n (for $n > 3$) compared to the ζ_n predicted by classical K41 scaling.

Instead of estimating ζ'_n directly from a regression fit of $S^{(n)}$ (hereafter called the direct estimate), Benzi et al. (1993b) suggested a method called extended self-similarity (ESS), where $\langle |\Delta u|^n \rangle$ is plotted against $\langle |\Delta u|^3 \rangle$. Since $\zeta'_n = \zeta_n = 1$ for $n = 3$, ζ'_n can be estimated directly by using a linear regression on a log–log plot. Benzi et al. (1993a) argued that the ESS method is more robust and the scaling range is larger compared with a fit of the inertial subrange using ''classical'' $\langle \Delta u^n \rangle$. Frisch (1995) points out that the ESS method ''gives much straighter graphs'' because the sampling undulations ''appear to be correlated among different orders of structure functions.'' Furthermore, ''the functional forms of the structure functions at the beginning of the dissipative fall-off are the same, down to about five times the Kolmogorov scale.'' Experiments (Shen and Warhaft 2002) have shown that ESS gives similar results to the direct method for low n. With ESS, they are able to determine ζ'_n for n up to 8, showing clearly the affects of intermittency.

3. Instrument overview

The helicopter-borne payload ACTOS as used to perform high-resolution measurements of turbulence and cloud microphysical parameters in stratocumulus clouds along the coast of the Baltic Sea around Kiel, Germany. ACTOS is an autonomous measurement system that is attached to a helicopter with a 140-m-long tether and carried with a true airspeed (TAS) of 15–20 m s^{-1}, which

is much lower than that of typical research aircraft, thereby yielding higher spatial resolution (assuming a constant sampling rate). A picture of ACTOS and a general introduction of the experimental setup are presented by Siebert et al. (2006a).

In addition to the standard equipment, a one-component hot-wire anemometer (HWA) was installed on ACTOS. The general use of a hot wire in (primarily artificial) clouds for turbulence measurements was discussed in Siebert et al. (2007). In this work, the same type of HWA is used as in that study. The HWA is based on a one-dimensional constant-temperature anemometer (CTA; type 54T30, Dantec Dynamics A/S, Skovlunde, Denmark) with a platinum-plated tungsten wire (type 55P01) of 5-μm diameter and an overall length of 3 mm, with the sensing part being 1.25 mm long. The bandwidth of the HWA is 10 kHz, but the raw signal is sampled only at 2192 Hz due to the limitations of the real-time data acquisition system of ACTOS (see also section 4).

For calibration of the hot-wire system, a three-dimensional ultrasonic anemometer (Solent HS, Gill Instruments, Lymington, United Kingdom) was used with a sampling frequency of 100 Hz. Ultrasonic anemometers have been shown not to be significantly affected by cloud droplets (Siebert and Teichmann 2000).

4. Despiking algorithm and postprocessing

In this section the algorithm used to remove spikes resulting from droplet impacts is introduced and evaluated (section 4a). The influence of despiking and averaging on nth-order structure functions is then analyzed by means of a drop-free dataset from an ACTOS flight with artificial spikes added.

a. Despiking and averaging

Under cloudy conditions, the signal of a hot-wire anemometer is significantly influenced by spikes due to impacting cloud droplets (e.g., Andreas et al. 1981). Based on wind-tunnel experiments, Siebert et al. (2007) showed that if the droplet number concentration is low and, therefore, the ratio between periods affected by spikes and drop-free periods is below a certain threshold, the spikes can be removed and the time series can be used for further analysis. In this work, a slightly modified despiking and interpolation algorithm is used.

The raw data were sampled with a frequency of f_s = 2192 Hz; a digital antialiasing filter at the input of the data acquisition system was set at $f_s/2$. However, under flight conditions with a low degree of turbulence, an oscillation with a sharp frequency around the Nyquist frequency ($f_{\mathrm{Ny}} = f_s/2$) was often observed that was not completely damped by the antialiasing filter. The aim of the "despiking algorithm" is therefore to detect the spikes and interpolate the affected data but also to remove the oscillation at f_{Ny}.

As a first step, the velocity increments (calculated as forward differences: $\Delta u_i \equiv u_{i+1} - u_i$) of the time series are calculated to distinguish between natural increments (due to natural turbulence) and spikes due to droplet impacts. Usually, the increments at the beginning of a droplet impact are sharp and about one order of magnitude greater than natural increments and, therefore, the spikes can be easily detected and distinguished from the natural turbulence. The typical duration of a spike (at a flow speed of 15 m s^{-1}) is on the order of 1 ms, that is, a few ($\sim$3) samples at a given f_s. A threshold-based despiking algorithm is used to detect the beginning of a spike. In parallel, a running median filter with a rank of 10 is applied to a copy of the same time series, which also removes the spikes as well as information on the small-scale turbulence in unaffected periods. Knowing the position of the beginning of a spike, the affected data (with a fixed length of five samples per spike) are removed and replaced by the elements of the filtered time series. This procedure is used iteratively up to 5 times to remove the remaining spikes that are due to coincidences or if an impaction event lasts longer than the typical five samples (e.g., big drops). Since the same threshold is applied, iterative use of this procedure does not affect drop-free periods. Finally, the data are decimated by applying nonoverlapping block averages over six elements to get a final sampling frequency of f_s = 365 Hz, which removes the aliasing effects but also small spikes remaining after the despiking procedure (e.g., tiny droplets or freshly activated aerosol).

The influence of the averaging and despiking on the statistics of velocity fluctuations and increments is analyzed to estimate the error introduced by the postprocessing. To that end, a 225-s-long record was selected, which was sampled in the atmosphere under drop-free conditions during a level flight at a height of 1.5 km under calm turbulence conditions. This data series was combined with artificial spikes of the same structure, amplitude, and duration as was observed for drop impaction in real clouds. The position of the artificial spikes was uniformly distributed and the average droplet–spike arrival time τ was set to 15 ms. Assuming a true airspeed of U = 15 m s^{-1} and a cross section of the hot wire (assuming a mean droplet diameter of 10 μm) of $\sigma = 2 \times 10^{-8}$ m^2 (Siebert et al. 2007), the average droplet–spike concentration N_d can be estimated to be $N_d = 1/(\tau\sigma U) \approx 200$ cm^{-3}. This is a value typically found for the marine stratocumulus clouds as observed during the analyzed Kiel 07 campaign.

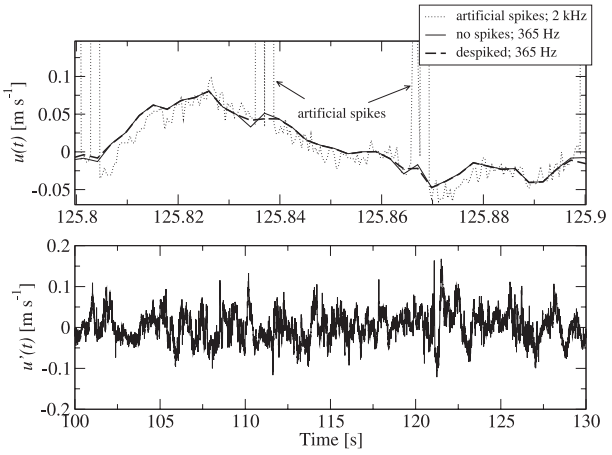

FIG. 1. (top) The influences of averaging and despiking for a 0.1-s-long (~1.5 m) subrecord chosen from a level flight in the residual layer ($z \approx 1.5$ km). The flight was under cloud-free conditions with weak turbulence. All data are calibrated and high-pass filtered at 0.5 Hz. The dotted curve shows hot-wire data sampled at 2192 Hz and with artificial spikes added. The number concentration (~200 cm^{-3}) of these spikes was similar to cloud droplet concentrations typically found in marine stratocumulus during this experiment. The thin solid line shows the same data without the artificial spikes but block averaged over six samples, resulting in a frequency of 365 Hz. The dashed line shows the data after the despiking and averaging algorithm was applied to the spiky raw data (dotted line). (bottom) The despiked and averaged data for a 450-m-long part of the subrecord.

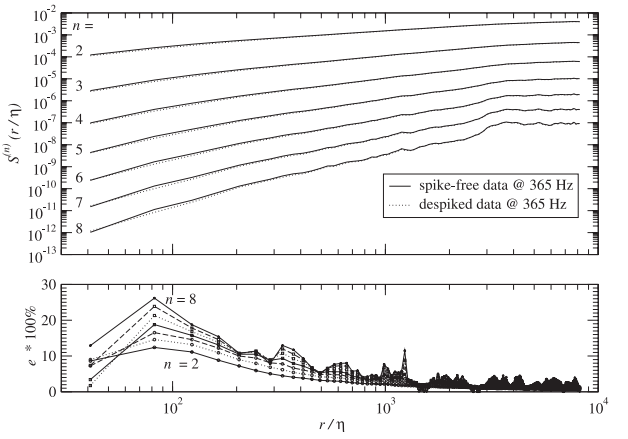

FIG. 2. The influences of averaging and despiking on $S^{(n)}$ for n = 2–8 are investigated. (top) The solid curves represent $S^{(n)}$ of the raw data (drop free), but already averaged over six samples, resulting in f_s = 365 Hz (reference case). The dotted curves are the same data but with artificial spikes added to the raw data (at f_s = 2192 Hz) and after the despiking and averaging algorithm was applied. (bottom) The relative error e of $S^{(n)}$ estimated from the despiked data with respect to the reference case. The relative error increases with increasing n and decreasing r/η; for $r/\eta \sim 80$; e is estimated to be about 10% (n = 2) to 30% (n = 8) and 2%–10% for $r/\eta > 10^3$.

A 0.1s-long section of the record, which corresponds to a flight path of 1.5 m, is shown in Fig. 1 (top). The thin solid curve represents the original (drop free) time series but averaged over six samples. This curve serves as a reference. The dotted line is the unfiltered time series at the original resolution (f_s = 2192 Hz), with artificial spikes added, and the thick-dashed curve is the result after applying the despiking and averaging algorithm on the dotted curve. The efficiency of the despiking algorithm for the few spikes shown in Fig. 1 can be seen at first glance. The bottom panel in Fig. 1 shows a 30-s-long part of the same flight leg through clear air, to which artificial droplet spikes were added followed by application of the despiking and averaging algorithm. The influence of the despiking algorithm on high-order structure functions will be analyzed in more detail in the following subsection.

b. *Influence of averaging and despiking on structure functions*

Structure functions behave differently compared with power spectra when using data influenced by noise or spikes. For example, noise with a certain frequency results in a more or less sharp peak in the spectrum but does not affect other frequencies, whereas the same noise would affect the entire structure function. Aliasing effects lead to an increase at the Nyquist frequency in a power spectrum whereas the entire structure function will be shifted toward larger values. To analyze the possible influence of intermittency effects on structure functions, it is essential to first carefully estimate the error due to the despiking and averaging algorithm. To understand how the structure functions will be influenced, we estimated $S^{(n)}(r/\eta)$ for n = 2–8 (see Fig. 2) using the same 225s-long record as is presented in Fig. 1. Here, $\eta \approx 1$ mm is the Kolmogorov length scale derived from a second-order structure function and the Kolmogorov 2/3 law [cf. Eq. (2)].

In the top panel of Fig. 2, the solid lines represent $S^{(n)}$ for the drop-free data, which were averaged before over six samples (f_s = 365 Hz). In the following, these curves are used as a reference. The dotted curves represents $S^{(n)}$ of the data (at original resolution) with artificial spikes but after the despiking and averaging algorithm was applied.

A small difference between the solid and dotted curves can be recognized for small values of r/η, which increases with increasing n. For $r/\eta > 10^3$, no differences are obvious in this plot. The bottom panel of Fig. 2 shows the relative error e of $S^{(n)}$ for the despiked data with respect to the reference case. The relative error increases with increasing n and decreasing r/η; for $r/\eta \sim 80$, e is at its maximum and is estimated to be from about 10% (n = 2) to 30% (n = 8) and 2% to 10% for $r/\eta > 10^3$.

This behavior has to be considered when discussing deviations from classical scaling in the next section.

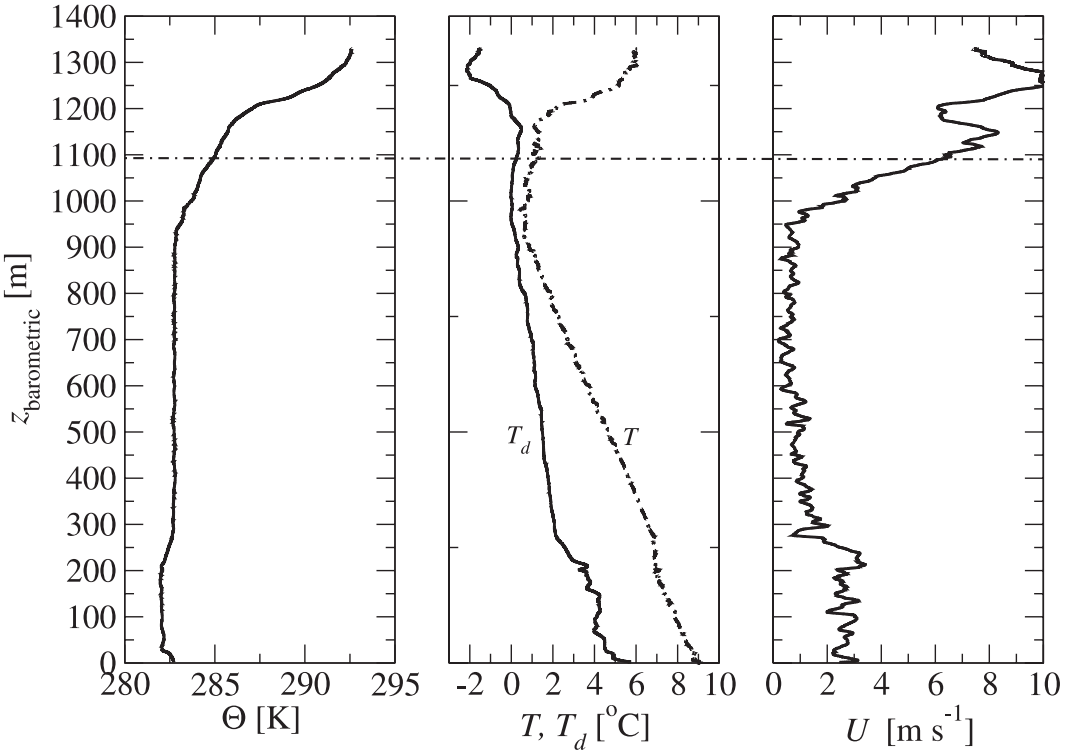

FIG. 3. Vertical profile of the potential temperature (Θ), temperature (T), dewpoint (T_d), and the horizontal wind speed (U). The profile was sampled directly after takeoff under cloud-free conditions. The dotted–dashed horizontal line at 1090 m indicates the height of the cloud measurements presented in Fig. 4.

Nevertheless, from these tests we conclude that, after despiking the drop-affected hot-wire data, a meaningful analysis of $\Delta u(x')$ with structure functions is possible.

5. Measurements in a marine stratocumulus layer

a. The experiment and meteorological conditions

During the Kiel 07 field campaign, which took place from 26 September to 10 October 2007, 11 helicopter flights from the Kiel Airport in Holtenau, near the German coast of the Baltic Sea, were performed. Typically, these flights started with a vertical profile under cloud-free conditions around the airport followed by several legs at constant height and flight direction. Depending on the local cloud situation, the horizontal legs were approximately 6 km long and flown along the mean wind direction. Since the helicopter had to remain outside the clouds, most cloud measurements were taken approximately 50–100 m below cloud top.

The present study is based on data taken on 10 October 2007. Takeoff was at 0700 UTC (0900 local time) and, after the ascent up to ~1.2 km, data were sampled in a field of stratocumulus clouds about 15 km off the coast. The analyzed flight leg (6 km long) was performed along the mean wind direction.

Figure 3 shows vertical profiles of potential temperature (Θ), temperature (T), dewpoint (T_d), and horizontal wind speed (U). The profiles start just after takeoff and were taken before the stratocumulus layer was reached over the Baltic Sea. Basically, above 290 m a well-mixed boundary layer was observed, characterized by a nearly uniform $\Theta \approx 283$ K, a slightly decreasing T_D from 2° to 0°C, and calm winds. This layer seems to be decoupled from the layer below, which might be caused by the difference between the boundary layer over land (just after takeoff up to ~300 m) and the layer above, which was gradually more influenced by the Baltic Sea as the coastline was approached. Above 950 m, a slight temperature inversion up to 1200 m with a vertical gradient of the potential temperature Θ of $\Gamma = \partial_z \Theta = +1.4 \times 10^{-2}$ K m^{-1} was observed. In this region, T_D was slightly increasing again. This inversion layer was followed by a much stronger inversion above 1200 m, with $\Gamma = +7 \times 10^{-2}$ K m^{-1} and decreasing T_D. The horizontal wind speed increased from 1 m s^{-1} in the well-mixed layer, up to 8–10 m s^{-1} in the inversion layer resulting in a strong horizontal wind shear. To answer the question of if the stable stratification ($\partial_z \Theta > 0$) allows sheer-induced turbulence to develop, we estimated the bulk Richardson number for this layer, which is defined by

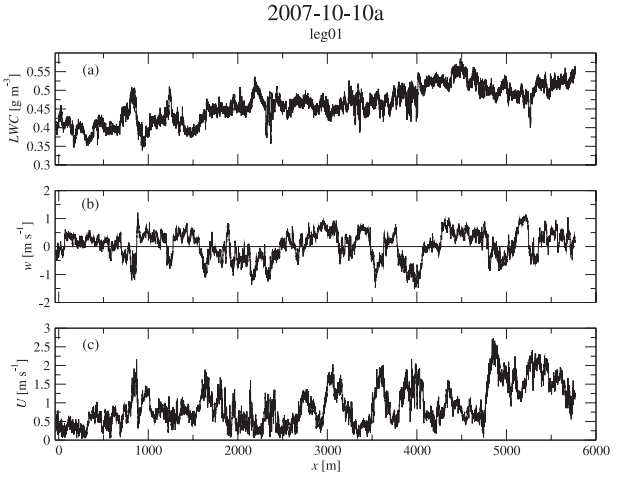

FIG. 4. Time series of (a) LWC, (b) the vertical velocity component (w), and (c) the horizontal wind velocity (U) of a 6-km-long (~6 min) leg in a stratocumulus layer. The data were sampled at a nearly constant height of 1090 m (a slow variation of the measurement height of ±10 m was present).

$$\mathrm{Ri} = \frac{g}{\overline{\Theta}} \frac{\Delta\Theta \Delta z}{\Delta \overline{U}^2}, \tag{4}$$

with $\Delta z = 200$ m, $\Delta\Theta = [\Theta(z = 1150\ \mathrm{m}) - \Theta(z = 950\ \mathrm{m})] \approx 2.7$ K, and $\Delta\overline{U} \approx 7\ \mathrm{m\ s^{-1}}$. Here, $\overline{\Theta}$ is the mean potential temperature in this layer and $g = 9.81\ \mathrm{m\ s^{-2}}$ is the acceleration due to gravity. From the profiles we estimate Ri ≈ 0.4, which is slightly above the critical value of $\mathrm{Ri}_c \approx 0.25$. This value of Ri allows only weak turbulence to develop.

There is another critical point to be considered: the maximum height of this profile was reached before the coastline and the cloud layer; that is, this profile might look slightly different over sea (and of course in the stratocumulus region) and the observed inversion height over land will slightly differ from the observed cloud top. That is, the Ri value estimated over land might be slightly different for the cloud area. Approaching the coastline, cloud top was observed at 1120 m above sea level and the vertical thickness of the cloud layer was estimated to be about 200 m.

Figure 4 presents the time history of several parameters to provide an overview of the 6-km-long (6 min) flight leg for which turbulence characteristics will be analyzed in detail. The leg was flown against the mean wind at a height of 1090 m, about 30 m below cloud top.

Figure 4a presents the liquid water content (LWC) measured with a Particle Volume Monitor [PVM-100A; see Gerber et al. (1994) for more details]. The LWC was slightly increasing from 0.4 to 0.5 g $\mathrm{m^{-3}}$ with increasing distance from the coast. The vertical velocity w (Fig. 4b) shows values of ±1.3 m $\mathrm{s^{-1}}$ with a mean value close to zero. The horizontal wind velocity U (Fig. 4c) was quite calm inside the cloud layer and ranges from ~0 to 2.5 m $\mathrm{s^{-1}}$. The vertical and horizontal wind velocities shown here were derived from the ultrasonic anemometer and were corrected for platform attitude and motion.

b. Calibration of the hot-wire system

The output signal E^2 of a hot-wire system is given by a function $f(u)$ of the flow velocity u and the difference between the wire and the ambient temperatures $(T_w - T_a)$ (Bruun 1995):

$$E^2 = f(u)(T_w - T_a). \tag{5}$$

In our setup, $T_w \approx 250$°C (at an overheat ratio of ~0.8) and T_a varies during the measurements between 0.3° and −0.2°C. Therefore, $(T_w - T_a)$ is assumed to be constant within less than 0.2% and no temperature corrections were applied.

The hot-wire anemometer was calibrated against the horizontal wind vector components, $u = \sqrt{u_s^2 + v_s^2}$ (with respect to a platform-fixed reference system) derived from the ultrasonic anemometer ("sonic"). Before calculating the sensitivity of the CTA, the sonic and CTA data were linearly detrended and a running median filter with rank 10 was applied to remove (i) spikes in the CTA signal due to droplet impaction and (ii) velocity fluctuations in the CTA data with scales below the spatial resolution of the sonic (~30 cm). The CTA electronics are based on a "mini-CTA" (Dantec, model 54T30) where the output is linearized and the electronics include basic signal conditioning. A linear regression through the scatterplot of the CTA output E' and the horizontal wind velocity fluctuations u' yields the sensitivity $a = \partial u/\partial E = 53.77\ \mathrm{m\ s^{-1}\ V^{-1}}$ (the detrended velocity and voltage residuals are denoted by primes).

c. Mean flow characteristics

From the longitudinal velocity component u and the vertical component w (derived from attitude-corrected ultrasonic anemometer data), the autocorrelation functions $\rho_u(r) = \overline{u'(x)u'(x+r)}/\sigma_u^2$ are calculated and the integral length scales $L_u = \int_0^\infty \rho_u(r)\, dr$ (e.g., Tennekes and Lumley 1972) are estimated. Integration of $\rho(r)$ from $r = 0$ to the first significant minimum of $\rho(r)$ [or the point where $\rho(r)$ crosses the x axis the first time] yields $L_u \approx L_w \approx 80$ m, whereas $\rho(L) = 1/e$ [assuming $\rho(r)$ has an exponential shape (see Kaimal and Finnigan 1994, for a discussion)] yields $L \approx 100$ m. From here on we will use $L \sim 100$ m, which is about half of the cloud layer thickness.

From the same time series we estimate $\sigma_u \approx 0.22\ \mathrm{m\ s^{-1}}$ and get $\overline{\varepsilon} = \sigma_u^3/L \approx 10^{-4}\ \mathrm{m^2\ s^{-3}}$. From a second-order structure function, we estimate $\overline{\varepsilon} = 2.94 \times 10^{-4}\ \mathrm{m^2\ s^{-3}}$ (this value is used in the text and for normalization of the

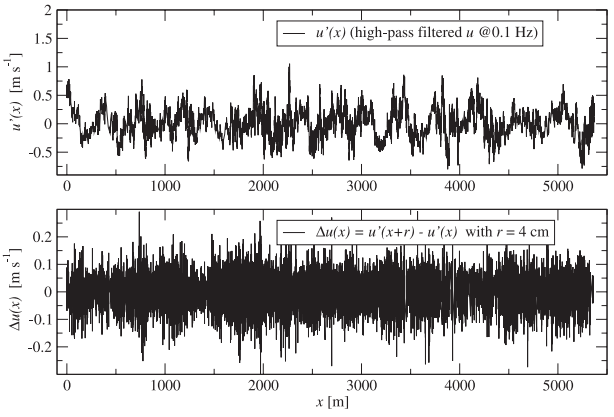

FIG. 5. Time series of (top) velocity fluctuations $u'(x)$ and (bottom) increments $\Delta u(x) = u'(x + r) - u'(x)$ (with fixed $r = 4$ cm) derived from despiked hot-wire data. The fluctuations u' are calculated by applying a high-pass filter (second-order Butterworth filter) with a cutoff frequency of 0.1 Hz corresponding to a wavelength of 150 m. The data are from the same record as for Fig. 4.

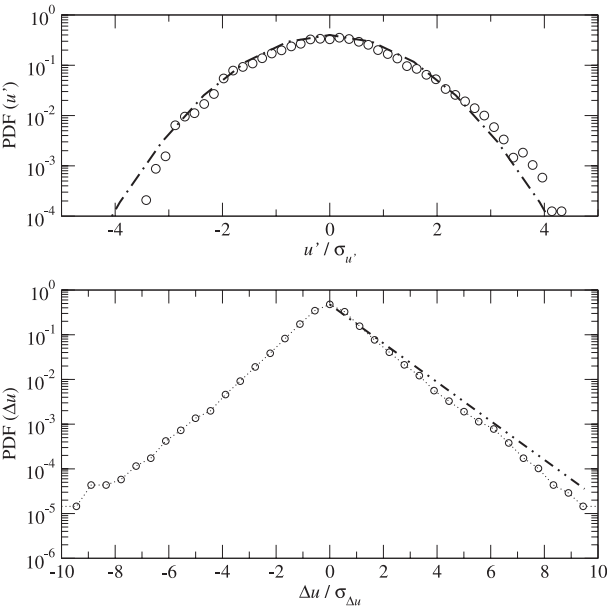

FIG. 6. The pdf's of the (top) velocity fluctuations u' and (bottom) increments Δu shown in Fig. 5. A Gaussian fit of pdf(u') and an exponential fit of the tails of pdf(Δu) are included for reference.

figures), which is in good agreement with the previous estimate. We estimate a Kolmogorov (dissipation) microscale of $\eta = (\nu^3/\overline{\varepsilon})^{1/4} \approx 1.8$ mm, for viscosity $\nu = 1.5 \times 10^{-5}$ m^2 s^{-1}.

We estimate a Taylor–Reynolds number of $\mathrm{Re}_\lambda = \sigma_u^2\sqrt{15/(\nu\overline{\varepsilon})} \sim 5 \times 10^3$. This value is about one order of magnitude smaller than the values found for cumulus clouds (Siebert et al. 2006b), which is in agreement with the general lower degree of turbulence expected in stratocumulus fields.

d. Hot-wire data analysis

1) PDF OF U' AND ΔU

For the same leg as shown in Fig. 4, we define velocity fluctuations $u'(x)$ and velocity increments $\Delta u(x) = u'(x + r) - u'(x)$ by applying a high-pass filter to the despiked hot-wire data $u(x)$. The filter cutoff is set at 0.1 Hz, corresponding to a length scale of 150 m, which is slightly above the integral length scale. This length is about 2–3 times the distance between the measurement height and cloud top and removes any influence from the pendulum motion of the ACTOS payload. Both time series are shown in Fig. 5 with $r = 4$ cm for the increments (spatial distance between two subsequent measurement points).

The intermittent character of these data is obvious: regions of relatively high and low fluctuations are found close to each other. The standard deviations of these high-pass-filtered data are $\sigma_{u'} \approx 0.23$ m s^{-1}, with peak values of around ± 1 m s^{-1}, and $\sigma_{\Delta u} \approx 0.03$ m s^{-1}, with peak values of $10\sigma_{\Delta u}$.

The intermittent character is further demonstrated through the pdf's of u' and Δu. At the large scales one would expect the fluctuations to be nearly Gaussian distributed. On the other hand, the velocity increments are affected by small-scale, intense events and, therefore, the pdf of Δu is highly non-Gaussian [see, e.g., discussions about velocity and increment pdf's in Frisch (1995) and Davidson (2004)]. In Fig. 6, the pdf's of u' (top panel) and Δu (bottom panel) are plotted. The x axes are normalized with the standard deviations $\sigma_{u'}$ and $\sigma_{\Delta u}$, respectively. For the pdf (u'), a Gaussian fit is included for comparison. There is slight skewness, possibly reflecting large-scale conditions. This level of skewness is also observed in well-controlled laboratory experiments (e.g., Mydlarski and Warhaft 1996, Fig. 5) and is remarkably low given the complex turbulent structure of the cloud at the large scales. The kurtosis of this pdf is $K = 3.2$, which is close to theoretical value of $K = 3$ for a Gaussian distribution. The pdf of Δu has a kurtosis of 8. The tails are approximately exponential (see fit line in Fig. 6b). This is consistent with observations in laboratory flows in the inertial subranges (e.g., Shen and Warhaft 2000, Fig. 16).

2) STRUCTURE FUNCTIONS

In section 2, the nth-order structure functions $S^{(n)}$ were introduced as a tool to describe the correlation of velocity increments. In Fig. 7, $S^{(n)}$ functions are presented for $n =$ 2–8 based on absolute increments $|\Delta u|$. The spatial lag r is normalized by the Kolmogorov length $\eta \approx 1.8$ mm.

At first glance, all functions qualitatively show an expected scaling behavior with power-law exponents increasing with increasing order. The scatter is due to the statistical sampling error, which increases with

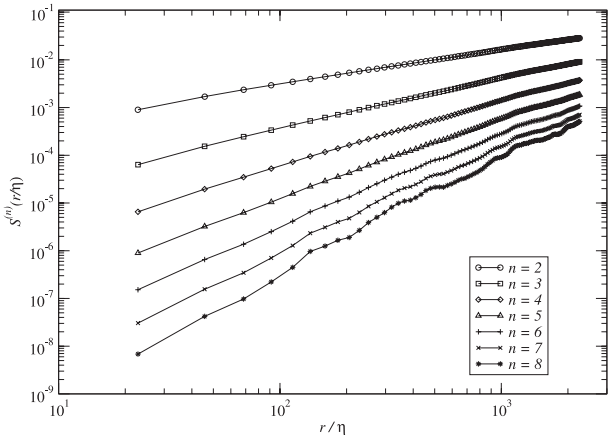

FIG. 7. The nth-order structure functions $S^{(n)}$ for $n = 2$–8 of the high-pass-filtered hot-wire data u' shown in Fig. 5. The spatial lag along the x axis is normalized with the Kolmogorov length $\eta = 1.8$ mm. The structure functions are derived from absolute values of the increments $|\Delta u|$.

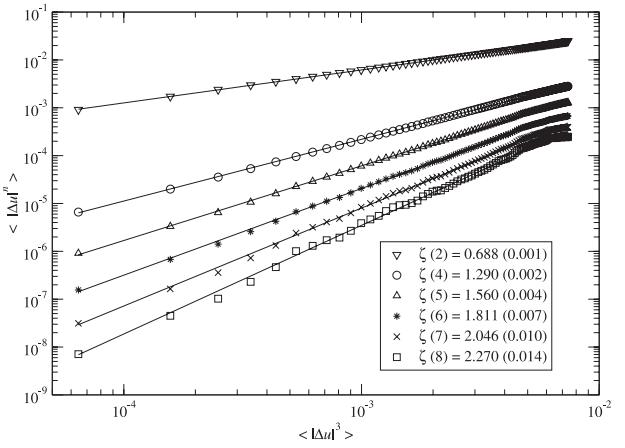

FIG. 8. The modulus of the nth-order structure functions $\langle|\Delta u|^n\rangle$ as a function of $\langle|\Delta u|^3\rangle$. The scaling exponents $\zeta(n)$ for $\langle|\Delta u|^n\rangle \sim \langle|\Delta u|^3\rangle^{\zeta(n)}$ are given in the plot for $n = 2$–8.

increasing order (see, e.g., Tennekes and Wyngaard 1972; Lenschow et al. 1994).

In Fig. 8, we plot the same structure functions as in Fig. 7 but as a function of $S^{(3)}$, as suggested by the ESS method (see section 2). The expected reduction in sampling fluctuations is apparent and this allows more accurate intermittency exponents to be obtained. The scaling exponents (ζ'_n) are estimated and given with their standard errors (in parentheses) of the least-square fit.

In Fig. 9, the scaling exponents are plotted as a function of n together with an estimate of the ζ'_n from a fit of $S^{(n)}$ in Fig. 8. Vertical error bars are included for the cloud measurements. The errors are estimated by varying the threshold for the despiking algorithm; an upper limit of the threshold was chosen such that small spikes are allowed to be undetected whereas a lower limit removed a few ''natural'' spikes. The classical K41 exponent $\zeta_n = n/3$ and the exponent including the intermittency correction (K62), together with values derived from well-controlled wind-tunnel experiments (Shen and Warhaft 2002), are included as a reference. For the cloud, data one can clearly see that for $n \geq 4$, the measured ζ'_n is below the classical $n/3$. The ESS method yields values quite close to the laboratory data and to the ''theoretical'' estimates [using a value of $\mu = 0.25$ taken from measurements; e.g., Sreenivasan and Kailasnath (1993)]. As mentioned previously, ESS provides a more extended inertial subrange than the direct method and, thus, a more reliable estimate of the scaling exponent. The results in Fig. 9 indicate that the turbulence in clouds is exhibiting intermittency effects similar to those observed in the laboratory in clear air. We note that the cloud-scaling exponents are slightly higher than those of the laboratory experiment. Laboratory and clear-air atmospheric experiments indicate that the scaling exponents are independent of Reynolds number (Sreenivasan and Antonia 1997) and boundary conditions (Jiang et al. 2006). Thus, we attribute the small variation to systematic error. Similar scatter is observed in the compilation of Sreenivasan and Antonia (1997, Fig. 3).

The normalized third- and fourth-order moments of Δu are the skewness function $\delta_S \equiv -S^{(3)}/(S^{(2)})^{3/2}$ and the kurtosis function $\delta_K \equiv S^{(4)}/(S^{(2)})^2$. For a pure Gaussian distribution $\delta_S = 0$ and $\delta_K = 3$, but at the small scales δ_S is slightly negative because of vortex stretching and $\delta_K > 3$ because of intermittency (Frisch 1995). At the large scales, δ_S and δ_K should approach the values of a normal distribution. Wyngaard and Tennekes (1970) give a range for $-\delta_S \in [0.5; 1]$ and $\delta_K \in [20; 50]$ for

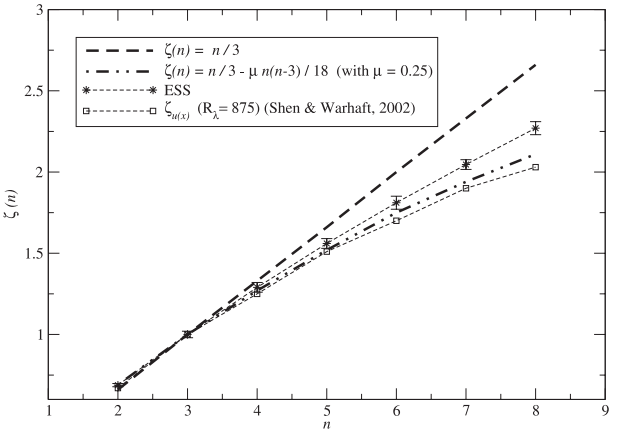

FIG. 9. The scaling exponents $\zeta(n)'$ of the structure functions, as plotted via ESS theory in Fig. 8. Theoretical values for K41 and for K62 with an intermittency factor of $\mu = 0.25$ are shown for reference, together with data derived from wind-tunnel experiments by Shen and Warhaft (2002).

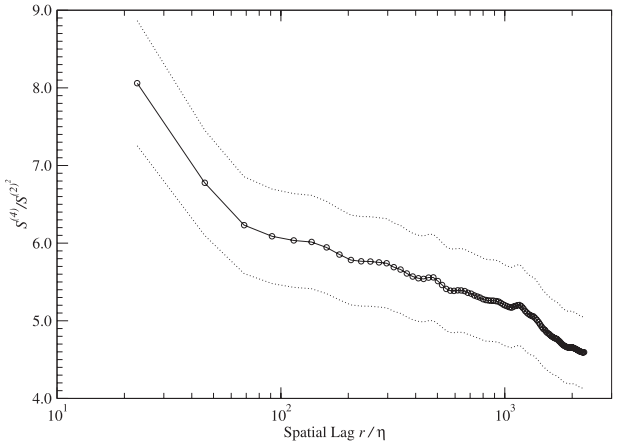

FIG. 10. Kurtosis function $K = S^{(4)}/(S^{(2)})^2$ as a function of the normalized lag r/η. The dotted lines indicate a $\pm 10\%$ range for the statistical sampling uncertainty (see text for more details).

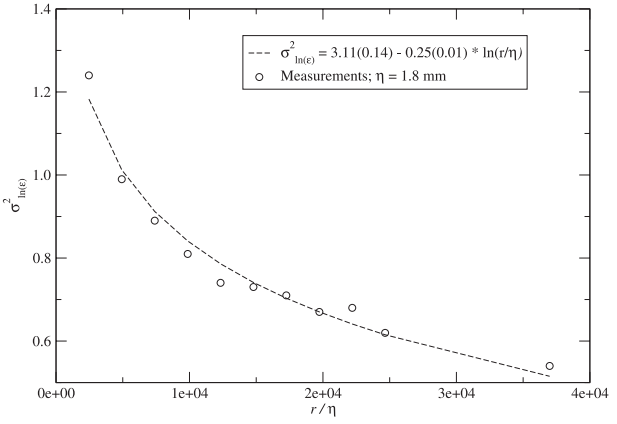

FIG. 11. Variance $\sigma^2_{\ln(\varepsilon_r)}$ as a function of the integration length r normalized with the Kolmogorov length $\eta \approx 1.8$ mm. An integral length scale of $L \approx 100$ m limits $r/\eta < L/\eta \approx 5 \times 10^4$. A logarithmic fit (dashed line) yields an intermittency exponent $\mu = 0.25$ with a standard error of 0.01.

atmospheric conditions for the first time derivative of the longitudinal velocity component, which indicates strong deviations from Gaussian. For wind-tunnel measurements in a shear flow (at somewhat lower Reynolds numbers compared to the atmosphere), Shen and Warhaft (2000) also observed significant deviations from Gaussian and an increasing δ_K with decreasing r. However, their δ_S values were smaller than those reported by Wyngaard and Tennekes (1970). In Fig. 10, $\delta_K(r)$ is plotted for the cloud data. The kurtosis function qualitatively shows increasing $\delta_K(r)$ as the dissipation scales are approached and a tendency toward Gaussian values for large r/η. The plot is consistent with the trend observed by Shen and Warhaft (2000, Fig. 14). Note that unlike the values of the structure function scaling exponents, this quantity increases with Reynolds number at the small scales (Sreenivasan and Antonia 1997).

It has to be pointed out that a statistically reliable estimate of the fourth moment requires very long sampling times. Following a strict criterion for the sampling error (e.g., Tennekes and Wyngaard 1972), the sampling time required to keep the sampling error below 10% (assuming a TAS = 18 m s^{-1}) would be on the order of 10^3 s, compared to our averaging time of approximately 360 s. To evaluate our sampling error, we make the following empirical estimate: we break the complete record into 10 subrecords of 540-m length each and estimate the kurtosis of each subrecord. The standard deviation ($\sigma_K \approx 0.9$) yields a relative error of about 10%, which is included as a dotted line in Fig. 10. The range of estimated K is [6.2: 9.1] with a mean of $K = 8$ (see also Fig. 6).

Taken together, these results show that internal intermittency is observed in cloud turbulence and that its effects on the structure functions are similar to those observed in the laboratory. To parameterize the intermittency, K62 and Obukhov (1962) recognized that $\Delta u(r)$ is not only influenced by the mean value of the dissipation, $\overline{\varepsilon}$, but also by its local value average over a distance r, ε_r. K62 conjectured that $\langle(\varepsilon_r)^2\rangle/\overline{\varepsilon}^2 \sim (L/r)^\mu \sim [(R_\lambda)^{3/2}(\eta/r)]$ in the inertial subrange. Here, μ is postulated to be a universal constant and is known as the intermittency exponent. If ε_r is log-normally distributed, it follows (e.g., Pope 2000) that the variance of $\ln(\varepsilon_r)$, $\sigma^2_{\ln(\varepsilon_r)}$ behaves as $\sigma^2_{\ln(\varepsilon_r)} = A - \ln(r/\eta)^\mu$. The local energy dissipation rate for this stratocumulus cloud is log-normally distributed (Siebert and Shaw 2008), and in Fig. 11 we plot $\sigma^2_{\ln(\varepsilon_r)}$ as a function of r/η. The fit to the data yields $\sigma^2_{\ln(\varepsilon_r)} = 3.11(0.14) - 0.25(0.01)$ $\ln(r/\eta)$ (standard deviations of the interpolation are given in trailing parentheses). The exponent of 0.25 is in remarkable agreement with the values of μ obtained in the laboratory and in the clear atmosphere (Praskovsky and Oncley 1994; Sreenivasan and Kailasnath 1993).

From Fig. 11, we also can obtain the variance of the energy dissipation rate at the Kolmogorov scale, $\sigma^2_{\ln(\varepsilon_r)|_\eta}$, even though it is not actually resolved directly; assuming a lognormal distribution of $\ln(\varepsilon)$, we can estimate an rms value of

$$\begin{aligned}\varepsilon'|_\eta &= \sqrt{\overline{\varepsilon}^2[\exp(\sigma^2_{\ln(\varepsilon_r)|_\eta}) - 1]} \\ &= \sqrt{(2.9 \times 10^{-4})^2(e^{3.11} - 1)\ \mathrm{m^2\,s^{-3}}} \\ &\approx 1.3 \times 10^{-3}\ \mathrm{m^2\,s^{-3}},\end{aligned}$$

given a mean value of $\overline{\varepsilon} = 2.9 \times 10^{-4}$.

The intermittency observed in the velocity increments and dissipation rates manifests itself in other ways that could be of relevance to cloud processes. For example, Lagrangian fluid accelerations play a role in cloud droplet

collision rates (e.g., Shaw and Oncley 2001; Pinsky and Khain 2004). With $a' = \varepsilon'^{3/4}\nu^{-1/4} \approx 0.1$ m s^{-2}, we have an rms value of fluid acceleration that is quite similar to that estimated using Hill's equation ($a_{\rm rms} \approx 0.17$ m s^{-2}) (Hill 2002). These values are compared to a mean Kolmogorov acceleration of $a_k \approx 0.04$ m s^{-2}. Furthermore, the tails of the Lagrangian acceleration pdf's have been shown to be exponential, displaying accelerations of $a = 10a_{\rm rms}$ with relative probability of 10^{-4} (Toschi and Bodenschatz 2009), which very well may be significant from the point of view of coalescence.

6. Summary and conclusions

High-resolution measurements of turbulence in a field of stratocumulus clouds have been presented. The measurements were performed close to cloud top in a 200-m-thick cloud layer on a flight path of approximately 6 km. The average degree of turbulence in terms of energy dissipation is relatively low ($\overline{\varepsilon} \sim 10^{-4}$ m^2 s^{-3}). Our analysis of the finescale structure of the turbulence is consistent with the picture that has been arrived at from a large body of laboratory studies, despite the difficulties inherent in performing the experiments in uncontrolled, multiphase conditions. Thus, we find that the scaling exponents of the higher-order structure functions indicate the presence of intermittency through their departure from the K41 prediction as the structure function order increases (Fig. 9). We determine the intermittency exponent of the turbulence to be 0.25 ± 0.01 (Fig. 11), consistent with the accepted value observed in the laboratory (e.g., Pope 2000; Davidson 2004). We find no evidence of any departure from the large body of knowledge obtained from the laboratory of the finescale turbulence structure. We note that while the turbulence Reynolds number in our cloud study is comparable to that observed at the higher end of laboratory studies ($R_\lambda \sim 10^3$), the dissipation rate is smaller by a few orders of magnitude than that typically observed in the laboratory.[2] It is the Reynolds number, however, that is the sole determining factor of the turbulence structure if stability effects are not strong.

Our observations that the finescale turbulence characteristics in clouds are similar to those observed in the laboratory suggest that turbulence quantities that we are not able at present to measure in clouds likely behave in a similar way in clouds as in the laboratory. In particular, the acceleration characteristics of fluid and inertial particles are determined by the underlying fluid field (Voth et al. 2002; Ayyalasomayajula et al. 2006). For fluid particles the Reynolds number is the sole determining flow parameter, but for inertial particles there are Stokes and Froude number effects. Recent laboratory experiments (Gerashchenko et al. 2008) show that the acceleration probability density functions have wide tails, with relatively slight attenuation at the Stokes and Froude numbers measured in clouds. Thus, the present results might be used in conjunction with laboratory measurement to predict droplet behavior in clouds (e.g., Saw et al. 2008). In general, this provides a great advantage for investigating detailed particle dynamics in laboratory chambers and wind tunnels.

The intermittent nature of turbulence in clouds is likely to influence processes involving scalar mixing or the local fluid field properties such as acceleration or shear. Ultimately, microphysical processes influenced by turbulence will interact with large-scale cloud properties, such as precipitation efficiency and radiative properties. Our study provides strong support for using well-established concepts of finescale turbulence structure for the study of these effects in clouds.

This study can be considered to be a first look at the microscale turbulence in clouds. The findings, therefore, should be interpreted within the context of the observed cloud properties: relatively low liquid water content and weak turbulent energy dissipation rate. Possible effects such as buoyancy reversal due to evaporative cooling and induced anisotropy on small scales may play a minor role in such clouds, but could influence the turbulence in deeper, more convective clouds (i.e., higher liquid water content and turbulence energy dissipation rate). It is important, therefore, to extend these measurements to other cloud types; statistically homogeneous fields of shallow cumulus clouds being one possibility.

Acknowledgments. We acknowledge Rolf Maser and Dieter Schell from the enviscope GmbH (Frankfurt am Main, Germany) for technical support and the two pilots, Alwin Vollmer and Oliver Schubert, from the rotorflug GmbH (Friedrichsdorf, Germany) for great helicopter flights. RAS acknowledges support from the Alexander von Humboldt Society and NSF Grant ATM-0535488 during the period in which this research was carried out. We thankfully acknowledge comments from J. C. Wyngaard and two anonymous reviewers who helped to improve the manuscript.

[2] In clouds, the high Reynolds numbers are achieved primarily because of the large scales ($R_\lambda \sim \varepsilon^{1/6}l^{2/3}/\nu^{1/2}$), while in the laboratory the scale is confined, but the dissipation is high.

REFERENCES

Andreas, E. L, R. M. Williams, and C. A. Paulson, 1981: Observations of condensate profiles over Arctic leads with a hot-film anemometer. *Quart. J. Roy. Meteor. Soc.,* **107,** 437–460.

Anselmet, F., Y. Gagne, E. J. Hopfinger, and R. A. Antonia, 1984: High-order velocity structure function in turbulent shear flows. *J. Fluid Mech.,* **140,** 63–89.

Ayyalasomayajula, S., A. Gylfason, L. R. Collins, E. Bodenschatz, and Z. Warhaft, 2006: Lagrangian measurements of inertial particle accelerations in grid generated wind tunnel turbulence. *Phys. Rev. Lett.,* **97,** 144507, doi:10.1103/PhysRevLett.97.144507.

Benzi, R., S. Ciliberto, C. Baudet, G. R. Chavarria, and R. Tripiccione, 1993a: Extended self-similarity in the dissipation range of fully developed turbulence. *Europhys. Lett.,* **24,** 275–279.

——, ——, ——, F. Massaioli, and S. Succi, 1993b: Extended self-similarity in turbulent flows. *Phys. Rev. E,* **48,** R29–R32.

Bruun, H. H., 1995: *Hot-Wire Anemometry*. Oxford University Press, 507 pp.

Crowe, C., M. Sommerfeld, and Y. Tsuji, 1997: *Multiphase Flows with Droplets and Particles*. Interpharm/CRC Press, 471 pp.

Davidson, P. A., 2004: *Turbulence*. Oxford University Press, 657 pp.

Frisch, U., 1995: *Turbulence—The legacy of A. N. Kolmogorov*. Cambridge University Press, 296 pp.

Gerashchenko, S., N. Sharp, S. Neuscamman, and Z. Warhaft, 2008: Lagrangian measurements of inertial particle accelerations in a turbulent boundary layer. *J. Fluid Mech.,* **617,** 255–281.

Gerber, H., B. G. Arends, and A. S. Ackerman, 1994: New microphysics sensor for aircraft use. *Atmos. Res.,* **31,** 235–252.

Haugen, D., Ed., 1973: *Workshop on Micrometeorology*. Amer. Meteor. Soc., 392 pp.

Hill, R. J., 2002: Scaling of acceleration in locally isotropic turbulence. *J. Fluid Mech.,* **452,** 361–370.

Ishihara, T., T. Gotoh, and Y. Kaneda, 2009: Study of high-Reynolds number isotropic turbulence by direct numerical simulation. *Annu. Rev. Fluid Mech.,* **41,** 165–180.

Jiang, X. Q., H. Gong, J. Liu, M. D. Zhou, and Z. S. She, 2006: Hierarchical structures in a turbulent free shear flow. *J. Fluid Mech.,* **569,** 259–286.

Kaimal, J. C., and J. J. Finnigan, 1994: *Atmospheric Boundary Layer Flows*. Oxford University Press, 289 pp.

Kolmogorov, A. N., 1941: The local structure of turbulence in incompressible viscous fluid for very large Reynolds numbers. *Dokl. Akad. Nauk SSSR,* **30,** 299–303.

——, 1962: A refinement of previous hypotheses concerning the local structure of turbulence in a viscous incompressible fluid at high Reynolds number. *J. Fluid Mech.,* **13,** 82–85.

Korczyk, P., S. P. Malinowski, and T. A. Kowalewski, 2006: Mixing of cloud and clear air in centimeter scales observed in laboratory by means of particle image velocimetry. *Atmos. Res.,* **82,** 173–182.

Lenschow, D. H., J. Mann, and L. Kristensen, 1994: How long is long enough when measuring fluxes and other turbulence statistics. *J. Atmos. Oceanic Technol.,* **11,** 661–673.

Malinowski, S. P., M. Andrejczuk, W. W. Grabowski, P. Korczyk, T. A. Kowalewski, and P. K. Smolarkiewicz, 2008: Laboratory and modeling studies of cloud-clear air interfacial mixing: anisotropy of small-scale turbulence due to evaporative cooling. *New J. Phys.,* **10,** 075020, doi:10.1088/1367-2630/10/7/075020.

Muschinski, A., R. G. Frehlich, and B. B. Balsley, 2004: Small-scale and large-scale intermittency in the nocturnal boundary layer and the residual layer. *J. Fluid Mech.,* **515,** 319–351.

Mydlarski, L., and Z. Warhaft, 1996: On the onset of high-Reynolds-number grid-generated wind tunnel turbulence. *J. Fluid Mech.,* **320,** 331–368.

Obukhov, A. M., 1962: Some specific features of atmospheric turbulence. *J. Geophys. Res.,* **67** (8), 3011–3014.

Pinsky, M. B., and A. P. Khain, 2004: Collision of small drops in a turbulent flow. Part II: Effects of flow accelerations. *J. Atmos. Sci.,* **61,** 1926–1939.

Pope, S. B., 2000: *Turbulent Flows*. Cambridge University Press, 771 pp.

Praskovsky, A., and S. Oncley, 1994: Probability density distribution of velocity differences at very high Reynolds numbers. *Phys. Rev. Lett.,* **73,** 3399–3402.

Saw, E. W., R. A. Shaw, S. Ayyalasomayajula, P. Y. Chuang, and A. Gylfason, 2008: Inertial clustering of particles in high-Reynolds-number turbulence. *Phys. Rev. Lett.,* **100,** 214501, doi:10.1103/PhysRevLett.100.214501.

Shaw, R. A., 2003: Particle–turbulence interactions in atmospheric clouds. *Annu. Rev. Fluid Mech.,* **35,** 183–227.

——, and S. P. Oncley, 2001: Acceleration intermittency and enhanced collision kernels in turbulent clouds. *Atmos. Res.,* **59–60,** 77–87.

Shen, X., and Z. Warhaft, 2000: The anisotropy of small scale structure in high Reynolds number ($R_\lambda \sim 1000$) turbulent shear flow. *Phys. Fluids,* **12,** 2976–2989.

——, and ——, 2002: Longitudinal and transverse structure functions in sheared and unsheared wind-tunnel turbulence. *Phys. Fluids,* **14,** 370–381.

Shraiman, B. I., and E. D. Siggia, 2000: Scalar turbulence. *Nature,* **405,** 639–646.

Siebert, H., and U. Teichmann, 2000: The behaviour of an ultrasonic under cloudy conditions. *Bound.-Layer Meteor.,* **94,** 165–169.

——, and R. A. Shaw, 2008: The small-scale structure of turbulence in marine stratocumulus. *Proc. 15th Int. Conf. on Clouds and Precipitation,* Cancun, Mexico, International Commission on Clouds and Precipitation–International Association of Meteorology and Atmospheric Sciences, 2.3. [Available online at http://cabernet.atmosfcu.unam.mx/ICCP-2008/abstracts/Program_on_line/Oral_02/Siebert_extended.pdf.]

——, H. Franke, K. Lehmann, R. Maser, E. W. Saw, D. Schell, R. A. Shaw, and M. Wendisch, 2006a: Probing fine-scale dynamics and microphysics of clouds with helicopter-borne measurements. *Bull. Amer. Meteor. Soc.,* **87,** 1727–1738.

——, K. Lehmann, and M. Wendisch, 2006b: Observations of small-scale turbulence and energy dissipation rates in the cloudy boundary layer. *J. Atmos. Sci.,* **63,** 1451–1466.

——, ——, and R. A. Shaw, 2007: On the use of a hot-wire anemometer for turbulence measurements in clouds. *J. Atmos. Oceanic Technol.,* **24,** 980–993.

Sreenivasan, K. R., and P. Kailasnath, 1993: An update on the intermittency exponent in turbulence. *Phys. Fluids A,* **5,** 512–514.

——, and R. A. Antonia, 1997: The phenomenology of small-scale turbulence. *Annu. Rev. Fluid Mech.,* **29,** 435–472.

Tanaka, T., and J. K. Eaton, 2008: Classification of turbulence modification by dispersed spheres using a novel dimensionless number. *Phys. Rev. Lett.,* **101,** 114502, doi:10.1103/PhysRevLett.101.114502.

Tennekes, H., and J. L. Lumley, 1972: *A First Course in Turbulence*. The MIT Press, 300 pp.

——, and J. C. Wyngaard, 1972: The intermittent small-scale structure of turbulence: Data-processing hazards. *J. Fluid Mech.,* **55,** 93–103.

Toschi, F., and E. Bodenschatz, 2009: Lagrangian properties of particles in turbulence. *Annu. Rev. Fluid Mech.,* **41,** 375–404.

Voth, G. A., A. La Porta, A. M. Crawford, J. Alexander, and E. Bodenschatz, 2002: Measurement of particle accelerations in fully developed turbulence. *J. Fluid Mech.,* **469,** 121–160.

Warhaft, Z., 2000: Passive scalars in turbulent flows. *Annu. Rev. Fluid Mech.,* **32,** 203–240.

Wyngaard, J. C., 2010: *Turbulence in the Atmosphere*. Cambridge University Press, 408 pp.

——, and H. Tennekes, 1970: Measurements of the small-scale structure of turbulence at moderate Reynolds numbers. *Phys. Fluids,* **13,** 1962–1969.